European Journal of Radiology 110 (2019) 249–255

Contents lists available at ScienceDirect

European Journal of Radiology

journal homepage: www.elsevier.com/locate/ejrad

Multiple mathematical models of diffusion-weighted magnetic resonance imaging combined with prognostic factors for assessing the response to neoadjuvant chemotherapy and radiation therapy in locally advanced rectal cancer

Chun-Yi Liang[a,1], Mao-Dong Chen[b,1], Xi-Xi Zhao[a], Cheng-Gong Yan[a], Ying-Jie Mei[b], Yi-Kai Xu[a,*]

[a] Department of Diagnostic Imaging Center, Nanfang Hospital, Southern Medical University, No. 1838 Guangzhou Avenue North, Guangzhou, Guangdong 510515, China
[b] School of Biomedical Engineering, Southern Medical University, No. 1838 Guangzhou Avenue North, Guangzhou, Guangdong 510515, China

ARTICLE INFO

Keywords:
DWI
Multiple mathematical models
Histogram analysis
Whole-tumor volume
Locally advanced rectal cancer
Response prediction

ABSTRACT

Purpose: To investigate whether the apparent diffusion coefficient (ADC), intravoxel incoherent motion (IVIM), and stretched exponential model (SEM) based on histogram analyses derived from the whole-tumor volume combined with prognostic factors can be used to assess the response to chemotherapy and radiation therapy (CRT) in locally advanced rectal cancer (LARC).

Materials and methods: This study included 60 patients with LARC who underwent diffusion-weighted imaging with 9b values (0–1000s/mm^2) before CRT. Histograms derived from the whole-tumor volume were used to obtain the ADC, IVIM (D_{slow}, D_{fast}, and f), and SEM parameters (distributed diffusion coefficient (DDC) and α). The histogram metrics and prognostic factors before CRT were compared between pathological complete response (pCR) and non-pCR patients. The receiver operating characteristic (ROC) and the area under the ROC curve (AUC) were generated to analyze the histogram metrics and prognostic factors.

Results: A significant difference was only found in the tumor volume between the pCR and non-pCR groups ($p = 0.033$, AUC = 0.740). The ADC mean, DDC median, and most of the histogram metrics were significantly lower in the pCR group than the non-pCR group ($p = 0.000–0.025$), and AUC was highest for the ADC mean (0.890). Only the D_{slow} median differed significantly between the two groups ($p = 0.023$, AUC = 0.721). However, the D_{fast}, f, and α histogram metrics did not differ significantly between the pCR and non-pCR groups. The AUC for the ADC mean combined with the tumor volume was 0.908, with a sensitivity of 100% and specificity of 81%. The inter-observer agreements were good or excellent for the ADC and SEM histogram parameters but generally fair for IVIM.

Conclusion: The whole-tumor ADC mean combined with the tumor volume was highly accurate for predicting pCR. The IVIM models were inferior to ADC and SEM at predicting pCR.

1. Introduction

Preoperative chemotherapy and radiation therapy (CRT) followed by surgical resection has been utilized as the standard therapeutic schedule for locally advanced rectal cancer (LARC) [1,2]. However, new data suggest that surgery may not be necessary in patients who achieve a pathological complete response (pCR) and these patients should be allocated to a “watch and wait” policy [3,4]. After a long course of preoperative CRT, approximately 5–45% of patients may achieve pCR [5,6]. By contrast, most of the remainder still exhibit tumor downstaging, no treatment response, and disease progression [7]. The early detection of poor responders may provide an opportunity to adjust the treatments for these patients, such as a higher radiation dose, second-line chemotherapy, or moving directly to surgery. Thus, predicting the treatment response is essential for individualizing LARC treatment according to good responders and poor responders. A method that can predict the therapeutic reaction before treatment would have significant clinical benefits. However, there are no reliable, noninvasive tests for predicting pCR.

Classic prognostic factors have been reported, including

* Corresponding author.
E-mail address: yikaivip@163.com (Y.-K. Xu).
[1] Chun-Yi Liang and Mao-Dong Chen were equally contribution to the study.

https://doi.org/10.1016/j.ejrad.2018.12.005
Received 23 August 2018; Received in revised form 25 October 2018; Accepted 4 December 2018

carcinoembryonic antigen (CEA), inflammatory cells, and tumor size [8–10]. Furthermore, pretreatment high-resolution magnetic resonance imaging (HR MRI) for rectal cancer is increasingly recommended because it allows preoperative identification of important surgical and pathological prognostic factors, such as the circumferential resection margin (CRM) and extramural venous invasion (EMVI) [11]. However, the conventional MRI sequence cannot give a reliable prediction of a tumor's response to CRT because it is difficult to differentiate the residual tumor from fibrosis induced by radiation [12] and it is not reliable for evaluating nodal involvement [13]. The conventional MRI sequence is insufficient for reliably addressing these critical challenges, so new techniques such as diffusion-weighted imaging (DWI) could potentially be employed to address this problem [14]. For example, several studies have identified associations between the apparent diffusion coefficient (ADC) values derived from DWI and rectal tumor response to CRT [15,16], whereas this association was not significant in other studies [14,17].

In a recent study, an intravoxel incoherent motion (IVIM) bi-exponential model that separates blood perfusion from true diffusion effects was shown to be widely applicable to tumors in the brain [18], lung [19], liver [20], kidney [21], and prostate [22]. This model is more detailed than the mono-exponential model, but the bi-exponential model exhibits poor repeatability and reproducibility [23]. Thus, the stretched exponential model (SEM) was used at high b values by Bennett et al. to overcome the inhomogeneity of tumor tissues [24]. Moreover, instead of using mean value measurements, histogram analysis based on the whole-tumor volume was employed to examine the heterogeneity in these studies [17,25]. There have been no previous applications of IVIM and SEM in rectal cancer. Given the value of whole-tumor volume IVIM metrics for characterizing other tumors, we hypothesize that this approach could be combined with prognostic factors for assessing the response of LARC to CRT.

Therefore, in this study, we explored the diagnostic performance of multiple mathematical models (ADC, IVIM, and SEM) according to histogram analyses derived from the whole-tumor volume combined with prognostic factors in order to assess the response of LARC to CRT by using the tumor regression grade (TRG) as the reference standard.

2. Materials and methods

Institutional review board approval was obtained from our hospital for this retrospective study and all patients gave written informed consent.

2.1. Patients

In total, 203 consecutive patients who received pre-CRT MRI examinations to evaluate rectal neoplasms at our department between October 2015 and November 2017 were enrolled in this single-institution study. Among these patients, 60 (mean age ± standard deviation = 54.63 ± 8.5 years) were selected according to the following inclusion criteria: (1) pathologically proven rectal adenocarcinoma; (2) underwent pretreatment MRI, including DWI with 9b values based on 3 T MRI for preoperative evaluation; (3) LARC (stage T3–T4) at pretreatment MRI; (4) no evidence of distant metastases; and (5) surgical resection 6–8 weeks after neoadjuvant CRT. Among the 203 patients, 143 were excluded because of the reasons listed in Fig. 1. Furthermore, all patients had CEA and routine blood tests before treatment.

2.2. Histopathologic TRG

All histopathologic examinations were performed by a team of pathologists who had more than 10 years of experience in rectal pathology. The tumor response to CRT was evaluated according to TRG as described by Dworak et al. [26]. Regression was from a complete response (grade 4) to no tumor regression (grade 0). Patients with TRG 4 were categorized as pathological complete response (pCR) with no tumor cells and only fibrotic mass (total regression or response), whereas TRG 0–3 were categorized as non-pCR.

2.3. MRI examination

All pre-CRT MRI examinations were performed with a Philips Achieva 3 T MR scanner (Philips Healthcare Inc, Best, The Netherlands) with a 16-channel SENSE-XL-Torso coil. The T2-weighted imaging

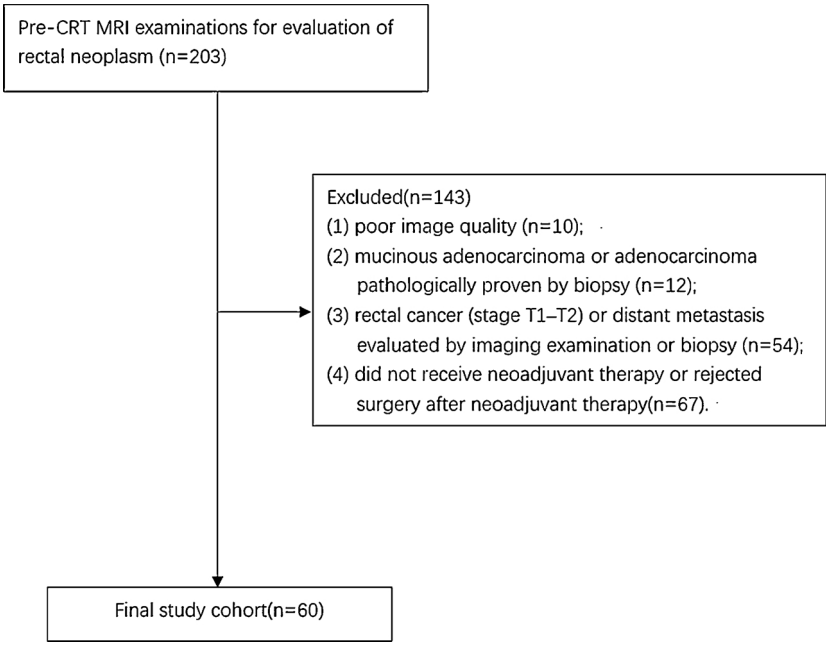

Fig. 1. Patient flow diagram.

(T2WI) data included the axial oblique, coronal, and sagittal planes. The axial oblique planes referred to as HR-T2WI were perpendicular to the long axis of the tumor in the sagittal plane. An axial HR-T2WI sequence was acquired with the following parameters: repetition time (TR) = 3906 ms, echo time (TE) = 100 ms, field of view (FOV) = 200 × 200 mm^2, voxel size = 0.63 × 0.63 × 3 mm^3, matrix size = 318 × 314, thickness = 3 mm, and number of signal averages (NSA) = 3, with 28 axial slices to cover the whole tumor without inter-slice gaps. Furthermore, a multiple-b DWI pulse sequence was obtained in the same orientation as the axial HR-T2WI imaging by using a single-shot echo-planar imaging pulse sequence with the following parameters: TR = 2000 ms, TE = 60 ms, FOV = 240 × 240 mm^2, voxel size = 2 × 2 × 4 mm^3, matrix size = 120 × 118, thickness = 3 mm with a gap of 0.4 mm, NSA = 3, and 9 b values (0, 10, 20, 40, 80, 150, 300, 600, and 1000s/mm^2). Finally, pre- and post-contrast axial T1-weighted imaging (T1WI) was performed before and after injecting the contrast media, followed by a 20 ml saline flush (15 mL Omniscan at a rate of approximately 4 mL/s using a power injector, and 20 mL of saline flush was injected at the same rate immediately afterward) with the following parameters: TR = 3.6 ms, TE = 1.35 ms, FOV = 342 × 260 mm^2, voxel size = 1.5 × 1.5 × 3 mm^3, matrix size = 228 × 172, thickness = 3 mm, and 133 slices axial with a gap of –1.5 mm.

During acquisition, the patients who were injected with 10 mg anisodamine hydrochloride (654-2) to prevent intestinal peristalsis half an hour before the scan were placed in a supine position in the gantry of the scanner and movement was limited. The total acquisition time was about 30 min, including the multiple-b DWI pulse sequence, which lasted 8 min.

2.4. Histogram analyses and volume measurements

The ADC, IVIM (D_{slow}, D_{fast}, and f), and SEM (distributed diffusion coefficient (DDC) and α) maps were generated with an in-house developed program, where they were fitted on a voxel-by-voxel basis using the nonlinear Levenberg-Marquardt method with the following multiple mathematical models.

1 Mono-exponential model: $S(b)/S(0) = \exp(-b \times ADC)$, where b is the level of diffusion weighting. ADC was calculated from a mono-exponential fit using 9 b values (0, 10, 20, 40, 80, 150, 300, 600, and 1000s/mm^2).
2 Bi-exponential model: $S(b)/S(0) = f \times \exp(-b \times D_{fast}) + (1 - f) \times \exp(-b \times D_{slow})$, where f is the diffusion fraction linked to microcirculation, which is also called the perfusion fraction, D_{fast} is the fast diffusion rate constant, and D_{slow} is the slow diffusion rate constant.
3 SEM: $S(b)/S(0) = \exp\{(-b \times s)^{\alpha}\}$, where DDC is a measure of the mean intravoxel diffusion rate in the presence of heterogeneity and the heterogeneity index α characterizes the deviation of the signal attenuation from mono-exponential form, which is limited to values between zero and one.

Two radiologists who were blinded to the clinical and pathological details, (XXX with 7 years of experience in abdominal MRI and XXX with 4 years of experience in oncologic body imaging) independently positioned a whole-tumor volume of interest (VOI) by manually enclosing the lesion in each HR-T2WI axial slice using commercially available software (TK-SNAP, version 3.4). In addition, VOIs were outlined in the DWI with a b-value of 1000s/mm^2 by referring to the HR-T2WI. Areas containing air, vessels, and artifacts were avoided when positioning the VOI.

The software automatically copied and pasted the VOIs derived from DWI images onto all the other maps mentioned above. Histograms were calculated from the VOIs in order to assess the distribution of parameters in the whole tumor and the following parameters were calculated: mean, minimum, maximum, standard deviation (SD), skewness, kurtosis, and the 5th, 10th, 25th, 75th, 90th, and 95th percentiles for ADC, D_{slow}, D_{fast}, f, DDC, and α (Fig. 2). Moreover, each tumor volume was automatically calculated by summing each of the axial slice volumes (axial slice area × slice thickness) derived from VOI of HR-T2WI with the same dedicated software, and the final value was the average determined by the two radiologists. In addition, CRM and EMVI were recorded according to the MRI report.

2.5. Statistical analyses

Statistical analyses were performed using a statistical software package (SPSS, version 22). The inter-observer variability in the tumor volume and histogram parameters were analyzed based on intraclass correlation coefficients (ICCs: 0.00–0.20 = poor correlation; 0.21–0.40 = fair; 0.41–0.60 = moderate; 0.61–0.80 = good; and 0.81–1.00 = excellent). Continuous variables were represented as the mean ± SD and compared with the Student's *t*-test or Mann–Whitney U test. Categorical variables were expressed as counts and compared using the χ^2-test or Fisher's exact test. Receiver operating characteristic (ROC) curve analysis was performed to analyze the histogram metrics and prognostic factors in order to evaluate their diagnostic accuracy for predicting pCR. The parameters were selected by multiple logistic regression analysis to assess the utility of adding the results obtained for prognostic factors to histogram analysis parameter. The selected parameters were combined by binary logistic regression analysis, which was used to obtain a generalized linear model, as shown in Eq. (1). The prediction probabilities(p) were calculated according to regression equations and the corresponding probability was used as an additional parameter, which was further assessed by ROC analysis. Moreover, the best cut-off was selected in terms of the sensitivity and specificity. Analyses were two-sided and differences were considered significant at $p < 0.05$.

$$\ln(p/(1-p)) = \beta_0 + \beta_1 x_1 + \ldots + \beta_m x_m \quad (1)$$

3. Results

Patient demographic data, the radiological stages based on pre-CRT MRI, and the pathological stages are shown in Table 1. After surgery, 13/60 patients achieved pCR (TRG0 = 21.7%), whereas the other 47 patients were classified according to the non-pCR group (TRG1–4 = 73.8%).

In terms of the reproducibility, the ICCs for the ADC and SEM histogram parameters obtained from pre-CRT had good or excellent correlations. However, the ICCs for IVIM mostly indicated fair correlations (Table 2).

3.1. Prediction and diagnostic performance of response: prognostic factors

None of the laboratory examination parameters (CEA and leukocytes) obtained before treatment differed significantly between the pCR and non-pCR groups (Table 1).

The mean tumor volume was 19.93 cm^3 (range = 3.38–98.41 cm^3) and there was a significant difference between the pCR (11.50 ± 6.93 cm^3) and non-pCR groups (22.26 ± 17.32 cm^3, $p = 0.033$). In addition, the AUC for the tumor volume parameter to predict pCR was 0.740 ($p = 0.009$, 95% confidence interval (95% CI) = 0.600–0.880), with a sensitivity of 84.6% and specificity of 57.4%.

According to pre-CRT MRI, mrCRM + was found in the images for 28/60 patients and there was no significant difference between the two groups. In terms of mrEMVI, mrEMVI + was slightly higher in the non-pCR group compared with the pCR group, but the difference was not significant ($p = 0.755$), and further details are shown in Table 1.

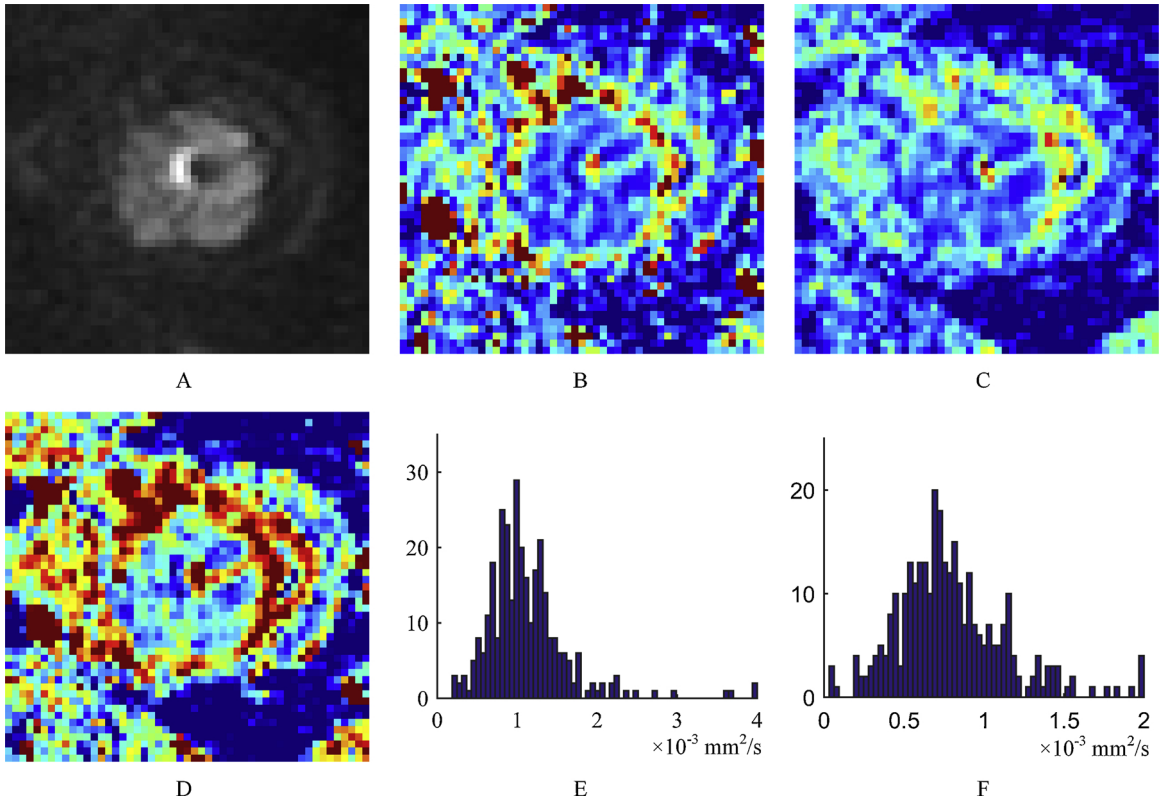

Fig. 2. T3N2 rectal cancer with pathological complete response based on pre-CRT MRI images, including DWI (a), ADC map (b), D_{slow} (c), and DDC map (d). Regions of interest were manually circumscribed in DWI. Graphs show the corresponding ADC histogram (e) and DDC histogram (f).

3.2. Prediction and diagnostic performance of response: histogram analyses

Tables 3 and 4 show the histogram parameters for the whole lesions (mean, median, variance, skewness, kurtosis, and 5th, 10th, 25th, 75th, 90th, and 95th percentiles) for the ADC, D_{slow}, D_{fast}, f, DDC, and α metrics in the cohort subsets.

The ADC mean, median, SD, and 10th, 25th, 75th, 90th, and 95th percentiles were significantly lower in the pCR group than the non-pCR group (p = 0.001–0.025). Table 5 shows that the highest diagnostic performance was obtained for the ADC mean (AUC = 0.890, p = 0.000, 95% CI = 0.806–0.974) with a sensitivity of 100% and specificity of 70.2%, and the optimal cutoff was 1.15×10^{-3} mm^2/s.

All of the D_{slow} histogram parameter values were lower in the pCR group than the non-pCR group, but only the D_{slow} median differed significantly between the two groups (p = 0.032). ROC curve analysis showed that the D_{slow} median could differentiate pCR and non-pCR with a sensitivity of 84.6% and specificity of 61.7% (AUC = 0.721, p = 0.015, 95% CI = 0.584–0.858) at the optimal cutoff of 0.76×10^{-3} mm^2/s. Unfortunately, none of the D_{fast} and f histogram parameters differed significantly between the pCR and non-pCR groups.

The mean, median, skewness, kurtosis, and 25th, 75th, 90th, and 95th percentiles for the DDC maps were lower in the pCR group compared with the non-pCR group (p = 0.000–0.013). When these eight parameters were tested separately by ROC curve analysis, the AUC

Table 1
Demographic, laboratory examination, radiological, surgery, and pathology data for the patients.

Characteristic	ALL	Response to chemotherapy		p-value
		pCR(n = 13)	Non-pCR(n = 47)	
Patient sex: Men/Women	46/14	11/2	35/12	0.444
Age(y)	54.63 ± 8.5	54.31 ± 10.1	54.72 ± 8.1	0.386
Laboratory examination				
CEA(μg/ml)	14.76 ± 26.18	15.3 ± 28.86	14.4 ± 25.7	0.089
Leukocytes(10^9/L)	7.09 ± 2.14	7.6 ± 2.07	6.93 ± 2.16	0.294
Radiology(Pretreatment MRI)				
Location*(0-5.0 cm/5.1-10.0 cm/10.1-15 cm)	32/22/6	8/4/1	24/18/5	0.796
Tumor volume(cm^3)	19.93 ± 16.24	11.50 ± 6.93	22.26 ± 17.32	**0.033**
mrCRM(+/-)	28/32	6/7	22/25	0.967
mrEMVI(+/-)	24/36	5/8	22/25	0.755
mrT stage(3/4)	39/21	8/5	31/16	0.767
mrN stage(0/1/2)	0/6/54	0/2/11	0/4/43	0.465
Pathology				
TRG(4/3/2/1/0)	13/28/10/6/3	13/0/0/0/0	0/28/10/6/3	**0.000**
pT stage(0/1/2/3/4)	13/3/15/16/13	13/0/0/0/0	0/3/15/16/13	**0.000**
pN stage(0/1/2)	47/9/4	12/1/0	35/8/4	0.348

Note: pCR, pathological complete response; *Location: Distance of the tumor from the anus; Significant results are printed in bold.

Table 2
Inter-observer intra-class correlation coefficients between two readers for all of the values obtained by histogram analysis.

parameters	Mono-exponential	Bi-exponential (IVIM)			Stretched-exponential	
	ADC	D_{slow}	D_{fast}	f	DDC	α
Mean	0.82	0.65	0.54	0.56	0.84	0.81
Median	0.84	0.73	0.52	0.55	0.85	0.75
SD	0.81	0.62	0.40	0.48	0.84	0.80
5th percentile	0.74	0.68	0.55	0.53	0.81	0.75
10th percentile	0.76	0.60	0.47	0.51	0.77	0.76
25th percentile	0.80	0.70	0.53	0.50	0.80	0.84
75th percentile	0.82	0.63	0.45	0.53	0.78	0.71
90th percentile	0.74	0.59	0.56	0.55	0.84	0.72
95th percentile	0.79	0.62	0.50	0.51	0.74	0.81
Skewness	0.81	0.67	0.43	0.54	0.82	0.83
kurtosis	0.82	0.54	0.47	0.44	0.80	0.81

value for the DDC median (0.866, $p = 0.000$, 95% CI = 0.771–0.960) was highest, followed by that of the DDC mean, and the AUC value was lowest for the DDC 95th percentile. In terms of the α value, none of the histogram metrics differed significantly.

3.3. Diagnostic performance: histogram analyses combined with prognostic factors

The AUC value for the ADC mean, which had the highest diagnostic performance among the histogram parameters combined with the tumor volume, was 0.908, with a sensitivity of 100% and specificity of 81% (Fig. 3).

4. Discussion

To the best of our knowledge, few previous studies of rectal cancer DWI have used histogram analysis with multiple mathematical models [27], and none have directly assessed the diagnostic performance of DWI histogram analyses combined with clinical prognostic factors for rectal cancer.

We found that the mean values were better than or equal to the histogram metrics, as also shown in a previous study [28], thereby suggesting that the mean values may be suitable for use in everyday clinical practice. In the present study, ADC histogram analysis based on pre-CRT MRI could discriminate pCR from non-pCR. In particular, the ADC mean value obtained from the pre-CRT ADC histogram had the best diagnostic performance according to histogram analysis. A recent study also that suggested a low pre-CRT ADC was helpful for detecting pCR [10]. It is possible that tumors with low pre-CRT ADC values are likely to be less necrotic with a higher cell density than those with high ADC values. It has been demonstrated that regions with a high cell density within a tumor may be associated with greater tissue perfusion, thereby resulting in better delivery and retention of chemotherapeutic drugs in these areas and a higher response to chemotherapy [29]. With the exception of the DWI parameters from the mono-exponential model, the DDC values derived from SEM histogram analysis could also differentiate the responders. Similar to a previous study [30], we found that a lower pre-CRT DDC was probably linked with pCR. We suggest that the association between a high DDC and more necrotic, less viable lesions is the same as a high ADC, which indicates that DDC can be interpreted in the same manner as ADC within the microenvironment. There was no significant difference in the diffusion index α between the pCR and non-pCR groups, but lower values were obtained for non-responsive lesions. A lower α value indicates vascular heterogeneity and the presence of microscopic necrosis, thereby making it more aggressive and less sensitive to chemotherapy [28].

Our results showed that the whole-tumor ADC mean combined with the tumor volume obtained the highest AUC values and this could be a promising method for predicting pCR. Consistent with previous studies [10,31], a smaller tumor size was a clinical predictor of achieving pCR, possibly because large tumors are linked with an increased risk of lymph node-positivity and metastases, and thus a poor prognosis [28]. However, using the tumor size alone to assess the tumor response to CRT is inadequate. Bakke [32] found that combining the f value with the tumor volume could significantly predict the tumor response, but they did not assess the diagnostic performance. However, we did not find that adding laboratory indexes (CEA and leukocytes) enhanced the prediction of the prognosis, unlike Giessen et al. [8], and this discrepancy might have occurred because only T3 and T4 were included in our cohort, thereby leading to selection bias. In contrast to a previous study [33], we found that mrCRM and mrEMVI had limited use in predicting a tumor's response to CRT, possibly because they are subjective parameters and susceptible to inter-observer variation.

We also found that the bi-exponential IVIM model performed worse compared with the mono-exponential model and SEM (DDC value) derived from the whole lesion in terms of predicting pCR as well as the reproducibility. In recent years, IVIM models have been used widely to evaluate the response of tumors to therapy [18–22], but f and D_{fast} derived from the IVIM model had inferior reproducibility according to the inter-observer variability test in our study. In order to improve the repeatability and stability, we used whole lesion analysis, where we considered the entire tumor to capture the inherent tumor heterogeneity and we used 9b values to capture the various diffusion

Table 3
Differences in histogram analyses of apparent diffusion (ADC) and stretched-exponential model (DDC and α) maps between the pathological complete response (pCR) and non-pCR groups.

parameters	ADC(10^{-3} mm^2/s)		p-value	DDC(10^{-3} mm^2/s)		p-value	α		p-value
	pCR (n = 13)	non-pCR (n = 47)		pCR (n = 13)	non-pCR (n = 47)		pCR (n = 13)	non-pCR (n = 47)	
Mean	1.04 ± 0.07	1.22 ± 0.18	**0.001**	0.78 ± 0.07	0.93 ± 0.16	**0.001**	0.70 ± 0.04	0.69 ± 0.05	0.964
Median	0.97 ± 0.06	1.14 ± 0.18	**0.001**	0.71 ± 0.06	0.88 ± 0.19	**0.000**	0.69 ± 0.06	0.68 ± 0.07	0.741
SD	0.39 ± 0.08	0.49 ± 0.14	**0.025**	0.32 ± 0.06	0.35 ± 0.08	0.132	0.20 ± 0.03	0.19 ± 0.03	0.334
5th percentile	0.53 ± 0.11	0.61 ± 0.17	0.145	0.38 ± 0.09	0.42 ± 0.17	0.121	0.37 ± 0.06	0.39 ± 0.06	0.325
10th percentile	0.63 ± 0.09	0.73 ± 0.14	**0.017**	0.45 ± 0.66	0.54 ± 0.15	0.054	0.43 ± 0.06	0.44 ± 0.07	0.574
25th percentile	0.78 ± 0.07	0.92 ± 0.13	**0.001**	0.57 ± 0.06	0.69 ± 0.14	**0.002**	0.54 ± 0.05	0.54 ± 0.07	0.899
75th percentile	1.22 ± 0.09	1.43 ± 0.27	**0.006**	0.92 ± 0.09	1.10 ± 0.22	**0.002**	0.87 ± 0.07	0.87 ± 0.08	0.898
90th percentile	1.51 ± 0.14	1.81 ± 0.36	**0.006**	1.20 ± 0.15	1.41 ± 0.24	**0.004**	0.99 ± 0.03	0.97 ± 0.06	0.513
95th percentile	1.73 ± 0.19	2.10 ± 0.44	**0.004**	1.42 ± 0.21	1.61 ± 0.25	**0.013**	1.00 ± 0.009	0.98 ± 0.03	0.264
Skewness	1.54 ± 0.50	1.63 ± 0.53	0.611	1.18 ± 0.09	0.76 ± 0.48	**0.000**	−0.06 ± 0.28	0.07 ± 0.24	0.454
kurtosis	8.44 ± 3.21	8.77 ± 3.19	0.734	5.21 ± 1.16	4.16 ± 1.25	**0.008**	2.16 ± 0.29	2.12 ± 0.35	0.663

Note: Significant results are shown in bold.

Table 4
Differences in histogram analyses of intravoxel incoherent motion (IVIM) maps between pathological complete response (pCR) and non-pCR groups.

parameters	$D_{fast}(10^{-3}mm^2/s)$		p-value	$D_{slow}(10^{-3}mm^2/s)$		p-value	f(%)		p-value
	pCR (n = 13)	non-pCR (n = 47)		pCR (n = 13)	non-pCR (n = 47)		pCR (n = 13)	non-pCR (n = 47)	
Mean	53.57 ± 7.03	54.93 ± 6.75	0.526	0.76 ± 0.05	0.84 ± 0.13	0.052	12.26 ± 2.60	12.68 ± 1.87	0.515
Median	23.60 ± 7.64	24.63 ± 7.67	0.669	0.73 ± 0.05	0.81 ± 0.13	**0.032**	11.63 ± 2.57	11.78 ± 2.15	0.841
SD	64.16 ± 4.72	64.99 ± 5.38	0.620	0.22 ± 0.04	0.25 ± 0.09	0.196	8.60 ± 1.56	9.42 ± 1.74	0.129
5th percentile	3.38 ± 1.00	3.02 ± 0.54	0.226	0.48 ± 0.08	0.47 ± 0.15	0.922	0.49 ± 1.21	0.10 ± 0.57	0.280
10th percentile	3.93 ± 2.31	3.49 ± 1.36	0.524	0.53 ± 0.07	0.56 ± 0.12	0.474	1.00 ± 2.25	0.84 ± 1.46	0.748
25th percentile	8.35 ± 4.36	8.37 ± 3.85	0.984	0.62 ± 0.06	0.68 ± 0.11	0.087	5.36 ± 2.88	5.09 ± 2.60	0.749
75th percentile	72.45 ± 18.47	76.42 ± 18.18	0.490	0.87 ± 0.06	0.98 ± 0.21	0.069	17.80 ± 3.27	18.54 ± 2.50	0.380
90th percentile	191.76 ± 14.44	189.67 ± 17.71	0.699	1.04 ± 0.08	1.16 ± 0.23	0.079	23.41 ± 3.98	25.10 ± 3.80	0.166
95th percentile	200 ± 0.00	199.94 ± 0.35	0.603	1.17 ± 0.11	1.29 ± 0.25	0.091	27.22 ± 4.65	29.61 ± 4.67	0.108
Skewness	1.41 ± 0.26	1.33 ± 0.23	0.365	0.89 ± 0.58	0.64 ± 0.61	0.210	0.65 ± 0.27	0.71 ± 0.24	0.405
kurtosis	3.65 ± 0.81	3.45 ± 0.73	0.402	5.54 ± 1.28	4.86 ± 1.19	0.133	3.67 ± 0.94	3.63 ± 0.71	0.886

Note: Significant results are shown in bold.

Table 5
Diagnostic performance of MRI histogram parameters.

MRI parameters	AUCs	p-value	Sensitivity(%)	Specificity(%)	Youden index	Cutoff value
ADC mean	**0.890**	0.000	100.0	70.2	0.70	1.15
ADC median	0.871	0.000	92.3	72.3	0.65	1.06
ADC SD	0.712	0.020	100.0	46.8	0.47	0.49
ADC 10th percentile	0.741	0.008	84.6	63.8	0.48	0.71
ADC 25th percentile	0.822	0.000	100.0	59.6	0.60	0.91
ADC 75th percentile	0.881	0.000	100.0	63.8	0.64	1.35
ADC 90th percentile	0.838	0.000	92.3	76.6	0.69	1.65
ADC 95th percentile	0.825	0.000	92.3	72.3	0.65	1.90
DDC mean	0.838	0.000	92.3	63.8	0.56	0.87
DDC median	**0.866**	0.000	100	63.8	0.64	0.80
DDC 25th percentile	0.818	0.000	100	66.0	0.66	0.64
DDC 75th percentile	0.827	0.000	92.3	61.7	0.54	1.03
DDC 90th percentile	0.763	0.004	92.3	48.9	0.41	1.38
DDC 95th percentile	0.718	0.017	76.9	63.8	0.41	1.55
DDC Skewness	0.825	0.000	92.3	78.7	0.71	1.07
DDC kurtosis	0.779	0.002	92.3	61.7	0.54	4.17
D_{slow} median	**0.721**	0.015	84.6	61.7	0.46	0.76

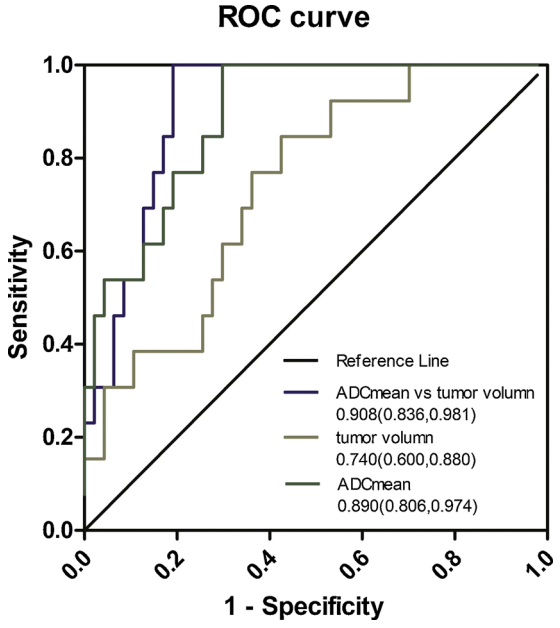

Fig. 3. Receiver operating characteristic (ROC) curve and the corresponding area under the ROC curve (AUCs) for parameters that significantly predicted the pathological complete response. Numbers in parentheses represent 95% confidence intervals.

properties of tissues. Unfortunately, the reproducibility was still poor for f and D_{fast}. These findings indicate that the models may be more sensitive to noise and artifacts [27], especially in the rectum, which is a hollow organ that contains gas and feces. By contrast, the mono-exponential model parameter ADC and the SEM parameter DDC were highly repeatable, which suggests that the parameters obtained from these two models are robust and they can be employed as reliable quantitative tools. Similarly, a previous study also showed that SEM obtained high ICC measures [30].

Our study had several limitations. First, our study cohort only included patients who received surgical resection after CRT, so selection bias was inevitable because our final binary outcome assessment of the response to CRT was defined according to the TRG. Second, we only focused on the response of the tumor to CRT and we neglected lymphadenopathy. Third, we did not analyze the post-CRT MR images, so further studies of both pre- and post-CRT MR images would be helpful for predicting the therapeutic response, which we plan to investigate. Finally, we performed DWI using 9 b-values (from 0 to 1000s/mm^2) but we did not evaluate the variability in the multi-b value DWI by performing repeated measurements, and we did not employ ADC measurements obtained from only 2 b-values (0 and 1000s/mm^2) used by Kim et al. [15]. In the further research, we will explore different b-value combinations to provide more valuable information.

In conclusion, we found that combining the whole-tumor ADC mean with the tumor volume was highly accurate at predicting the response of LARC to CRT. Furthermore, our preliminary results indicated that the mean value was better than or equal to histogram analysis, and thus the

mean value may be suitable for use in everyday clinical practice. Finally, according to our results, IVIM models were inferior to mono-exponential modeling and SEM in terms of predicting pCR as well as their reproducibility.

Fundings

This work was financially supported by the National Natural Science Foundation of China (No. 81871334), Science and Technology Planning Project of Guangdong Province, China (No. 2015B010131011), National Key Research and Development Program of China (No. 2016YFC0107104) and the Program for Changjiang Scholars and Innovative Research Team in University (No. IRT_16R37).

Conflict of interest

The authors declared that they have no conflicts of interest to this work, there is no professional or other personal interest of any nature or kind in any product, service and/or company that could be construed as influencing the position presented in, or the review of, the manuscript entitled.

References

[1] M. Mihmanlı, E. Kabul Gürbulak, İE. Akgün, et al., Delaying surgery after neoadjuvant chemoradiotherapy improves prognosis of rectal cancer, World J. Gastrointest. Oncol. 8 (9) (2016) 695.
[2] B.C. Chapman, P. Hosokawa, W. Henderson, et al., Impact of neoadjuvant chemoradiation on perioperative outcomes in patients with rectal cancer, J. Surg. Oncol. 115 (8) (2017) 1033–1044.
[3] A. Habr-Gama, J. Sabbaga, J. Gama-Rodrigues, et al., Watch and wait approach following extended neoadjuvant chemoradiation for distal rectal cancer, Dis. Colon Rectum 56 (10) (2013) 1109–1117.
[4] J.C. Kong, G.R. Guerra, S.K. Warrier, et al., Outcome and salvage surgery following "Watch and wait" for rectal cancer after neoadjuvant therapy: a systematic review, Dis. Colon Rectum 60 (3) (2017) 335–345.
[5] G. Dedemadi, S.D. Wexner, Complete response after neoadjuvant therapy in rectal cancer: to operate or not to operate? Dig. Dis. 30 (Suppl 2) (2012) 109–117.
[6] S. Nougaret, C. Reinhold, H.W. Mikhael, et al., The use of MR imaging in treatment planning for patients with rectal carcinoma: have you checked the "DISTANCE"? Radiology 268 (2) (2013) 330–344.
[7] A. Trakarnsanga, S. Ithimakin, M.R. Weiser, Treatment of locally advanced rectal cancer: controversies and questions, World J. Gastroenterol. 18 (39) (2012) 5521–5532.
[8] C. Giessen, D. Nagel, M. Glas, et al., Evaluation of preoperative serum markers for individual patient prognosis in stage I-III rectal cancer, Tumour Biol. 35 (10) (2014) 10237–10248.
[9] D. Hanahan, R.A. Weinberg, Hallmarks of cancer: the next generation, Cell 144 (5) (2011) 646–674.
[10] M.L. Garland, R. Vather, N. Bunkley, et al., Clinical tumour size and nodal status predict pathologic complete response following neoadjuvant chemoradiotherapy for rectal cancer, Int. J. Colorectal Dis. 29 (3) (2014) 301–307.
[11] G. Brown, A.G. Radcliffe, R.G. Newcombe, et al., Preoperative assessment of prognostic factors in rectal cancer using high-resolution magnetic resonance imaging, Br. J. Surg. 90 (3) (2003) 355–364.
[12] R.C. Dresen, M. Kusters, A.W. Daniels-Gooszen, et al., Absence of tumor invasion into pelvic structures in locally recurrent rectal cancer: prediction with preoperative MR imaging, Radiology 256 (1) (2010) 143–150.
[13] M.P. van der Paardt, M.B. Zagers, R.G.H. Beets-Tan, et al., Patients who undergo preoperative chemoradiotherapy for locally advanced rectal Cancer Restaged by using diagnostic MR imaging: a systematic review and meta-analysis, Radiology 269 (1) (2013) 101–112.
[14] L. Curvo-Semedo, D.M. Lambregts, M. Maas, et al., Rectal cancer: assessment of complete response to preoperative combined radiation therapy with chemotherapy–conventional MR volumetry versus diffusion-weighted MR imaging, Radiology 260 (3) (2011) 734–743.
[15] S.H. Kim, J.M. Lee, S.H. Hong, et al., Locally advanced rectal cancer: added value of diffusion-weighted MR imaging in the evaluation of tumor response to neoadjuvant chemo- and radiation therapy, Radiology 253 (1) (2009) 116–125.
[16] B. Barbaro, R. Vitale, V. Valentini, et al., Diffusion-weighted magnetic resonance imaging in monitoring rectal cancer response to neoadjuvant chemoradiotherapy, Int. J. Radiat. Oncol. Biol. Phys. 83 (2) (2012) 594–599.
[17] Y.C. Kim, J.S. Lim, K.C. Keum, et al., Comparison of diffusion-weighted MRI and MR volumetry in the evaluation of early treatment outcomes after preoperative chemoradiotherapy for locally advanced rectal cancer, J. Magn. Reson. Imaging 34 (3) (2011) 570–576.
[18] W.C. Wu, S.C. Yang, Y.F. Chen, et al., Simultaneous assessment of cerebral blood volume and diffusion heterogeneity using hybrid IVIM and DK MR imaging: initial experience with brain tumors, Eur. Radiol. 27 (1) (2017) 306–314.
[19] C. Yan, J. Xu, W. Xiong, et al., Use of intravoxel incoherent motion diffusion-weighted MR imaging for assessment of treatment response to invasive fungal infection in the lung, Eur. Radiol. 27 (1) (2017) 212–221.
[20] M. Klauss, P. Mayer, K. Maier-Hein, et al., IVIM-diffusion-MRI for the differentiation of solid benign and malign hypervascular liver lesions-Evaluation with two different MR scanners, Eur. J. Radiol. 85 (7) (2016) 1289–1294.
[21] B. Gaing, E.E. Sigmund, W.C. Huang, et al., Subtype differentiation of renal tumors using voxel-based histogram analysis of intravoxel incoherent motion parameters, Invest. Radiol. 50 (3) (2015) 144–152.
[22] Y.D. Zhang, Q. Wang, C.J. Wu, et al., The histogram analysis of diffusion-weighted intravoxel incoherent motion (IVIM) imaging for differentiating the gleason grade of prostate cancer, Eur. Radiol. 25 (4) (2015) 994–1004.
[23] H.A. Dyvorne, N. Galea, T. Nevers, et al., Diffusion-weighted imaging of the liver with multiple b values: effect of diffusion gradient polarity and breathing acquisition on image quality and intravoxel incoherent motion parameters–a pilot study, Radiology 266 (3) (2013) 920–929.
[24] R. Bedair, A.N. Priest, A.J. Patterson, et al., Assessment of early treatment response to neoadjuvant chemotherapy in breast cancer using non-mono-exponential diffusion models: a feasibility study comparing the baseline and mid-treatment MRI examinations, Eur. Radiol. 27 (7) (2017) 2726–2736.
[25] D. Genovesi, A. Filippone, C.G. Ausili, et al., Diffusion-weighted magnetic resonance for prediction of response after neoadjuvant chemoradiation therapy for locally advanced rectal cancer: preliminary results of a monoinstitutional prospective study, Eur. J. Surg. Oncol. 39 (10) (2013) 1071–1078.
[26] O. Dworak, L. Keilholz, A. Hoffmann, et al., Pathological features of rectal cancer after preoperative radiochemotherapy, Int. J. Colorectal Dis. 12 (1997) 19–23.
[27] H.B. Zhu, X.Y. Zhang, X.H. Zhou, et al., Assessment of pathological complete response to preoperative chemoradiotherapy by means of multiple mathematical models of diffusion-weighted MRI in locally advanced rectal cancer: a prospective single-center study, J. Magn. Reson. Imaging 46 (1) (2017) 175–183.
[28] S. Nougaret, H.A. Vargas, Y. Lakhman, et al., Intravoxel incoherent motion-derived histogram metrics for assessment of response after combined chemotherapy and radiation therapy in rectal Cancer: initial experience and comparison between single-section and volumetric analyses, Radiology 280 (2) (2016) 446–454.
[29] K.M. Bennett, K.M. Schmainda, R.T. Bennett, et al., Characterization of continuously distributed cortical water diffusion rates with a stretched-exponential model, Magn. Reson. Med. 50 (4) (2003) 727–734.
[30] R. Bedair, A.N. Priest, A.J. Patterson, et al., Assessment of early treatment response to neoadjuvant chemotherapy in breast cancer using non-mono-exponential diffusion models: a feasibility study comparing the baseline and mid-treatment MRI examinations, Eur. Radiol. 27 (7) (2017) 2726–2736.
[31] M. Lambrecht, V. Vandecaveye, F. De Keyzer, et al., Value of Diffusion-Weighted Magnetic Resonance Imaging for Prediction and Early Assessment of Response to Neoadjuvant Radiochemotherapy in Rectal Cancer: Preliminary Results, Int. J. Radiat. Oncol. 82 (2) (2012) 863–870.
[32] K.M. Bakke, K.H. Hole, S. Dueland, et al., Diffusion-weighted magnetic resonance imaging of rectal cancer: tumour volume and perfusion fraction predict chemoradiotherapy response and survival, Acta Oncol. 56 (6) (2017) 813–818.
[33] Tait D. Yu SK, I. Chau, et al., MRI predictive factors for tumor response in rectal cancer following neoadjuvant chemoradiation therapy–implications for induction chemotherapy? Int. J. Radiat. Oncol. Biol. Phys. 87 (3) (2013) 505–511.